Page Proof Instructions and Queries

Journal Title: JIM
Article Number: 963169

Thank you for choosing to publish with us. This is your final opportunity to ensure your article will be accurate at publication. Please review your proof carefully and respond to the queries using the circled tools in the image below, which are available in Adobe Reader DC* by clicking **Tools** from the top menu, then clicking **Comment**.

Please use *only* the tools circled in the image, as edits via other tools/methods can be lost during file conversion. For comments, questions, or formatting requests, please use T. Please do *not* use comment bubbles/sticky notes.

*If you do not see these tools, please ensure you have opened this file with **Adobe Reader DC**, available for free at get.adobe.com/reader or by going to Help > Check for Updates within other versions of Reader. For more detailed instructions, please see us.sagepub.com/ReaderXProofs.

Sl. No.	Query
	Please note that we cannot add/amend orcid ids for any article at the proof stage. following orcid's guidelines, the publisher can include only orcid ids that the authors have specifically validated for each manuscript prior to official acceptance for publication.
	Please confirm that all author information, including names, affiliations, sequence, and contact details, is correct.
	Please review the entire document for typographical errors, mathematical errors, and any other necessary corrections; check headings, tables, and figures.
	Please ensure that you have obtained and enclosed all necessary permissions for the reproduction of art works (e.g. illustrations, photographs, charts, maps, other visual material, etc.) not owned by yourself. please refer to your publishing agreement for further information.
	Please note that this proof represents your final opportunity to review your article prior to publication, so please do send all of your changes now.
	Please confirm that the funding and conflict of interest statements are accurate.
1	Please provide missing Article Type
2	Please check the hierarchy of below heading levels
3	Please supply missing Publisher location.
4	Please supply missing Journal title and Page range.
5	Please supply missing Volume number and Page range.
6	Reference "Li et al., 2013" is not cited in text. Please indicate where the respective citation should appear or allow us to delete the references.
7	Please supply missing Publisher location.
8	Please supply missing Publisher location.

Journal of
Intelligent Material
Systems and Structures

Journal of Intelligent Material Systems and Structures
1–12

DOI: 10.1177/1045389X20963169
journals.sagepub.com/home/jim
SAGE

Magnetorheological elastomers characterization under shear loading up to failure: A magneto-mechanical multivariate analysis[AQ: 1]

Andrea Spaggiari and Alberto Bellelli

Abstract

This work analyses the shear behavior of magnetorheological elastomers (MRE), a class of smart materials which presents interesting magneto-mechanical properties. In order to determine the effect of several variables at a time, a design of experiment approach is adopted. A set of several samples of MRE was manufactured, by varying the weight fraction of ferromagnetic material inside the viscoelastic matrix and the isotropicity of the material, by adding an external magnetic field while the elastomeric matrix was still liquid. The mechanical behavior of each sample was analyzed by conducting cyclic tests at several shear rates, both with and without an external magnetic field. Moreover, in order to estimate the maximum shear stress, the specimens were loaded monotonically up to failure. Shear stiffness, maximum shear stress and specific dissipated energy were calculated on the basis of the experimental data. The results were analyzed using an Analysis of Variance (ANOVA) to assess the statistical influence of each variable. The experimental results highlighted a strong correlation between the weight fraction of ferromagnetic material in each sample and its mechanical behavior. Moreover, the dissipated energy of the MRE drops down when the magnetic field stiffens the behavior or the shear rate increases. The ultimate failure shear stress is strongly affected by the external magnetic field, increasing it by nearly 50%. The ANOVA on the results provides a simple phenomenological model is built for each output variable and it is compared with the experimental tests. These models produce a fast and fairly accurate prediction of each analyzed response of the MRE under various shear rates and applied magnetic fields.

Keywords

Magnetorheological elastomers, characterization, ANOVA, shear stress

1. Introduction

The study of magnetorheological elastomers, smart materials whose properties are currently under-utilized for vibration suppression, could lead to a better understanding of the complex interactions between the several concurrent phenomena acting in the material, such as the viscoelastic behavior, the magnetic field dependence and the anisotropicity. So far, their use in practical application is still limited to some recent applications such as an automotive MRE mount (Kim et al., 2018), seismic applications (Eem et al., 2019) or a collection of potential applications as proposed in (Li and Zhang, 2012). MREs have also been patented by Ford Motor Company as a bearing for automotive applications, where the stiffness of this bearing is adjusted according to the state of the powertrain, in order to optimize the suspension thus improving passengers' comfort. It may be noted that although to date several applications that involve the use of anisotropic MREs have been patented, no industrial product is yet available on the market, probably since their performance still does not justify their costs and lack of complete information about durability and strength of these materials. It is quite peculiar that a commercial application of a particular sort of MRE is a material mainly sold as a toy, the so-called Silly Putty already studied by (Cross, 2012; Marc Hartzman, 2013), especially in its magnetic sensitive form, the Thinking

Department of Sciences and Methods for Engineering, University of Modena and Reggio Emilia, Reggio Emilia, Italy

Corresponding author:
Andrea Spaggiari, Department of Sciences and Methods for Engineering, University of Modena and Reggio Emilia, via Amendola, 2, Campus S. Lazzaro, Reggio Emilia 42122, Italy.
Email: andrea.spaggiari@unimore.it

Putty, (Golinelli et al., 2015). Silly Putty represents the "ideal" viscoelastic material, because it is incredibly stiff in case of high deformation rates, while it is very deformable and soft for quasi-static applied stress (Cross, 2012). However, its semi-fluid behavior makes Silly Putty unsuitable for engineering applications. Even though it was created to replace rubber seals its application is not possible, since it cannot keep a preformed shape and it also collapses under its own weight. Conversely the magnetorheological elastomers (MREs), which consist of ferromagnetic micrometric particles suspended in a non-magnetic elastomeric matrix (Davis, 1999; Guan et al., 2008; Ruddy et al., 2008) behave quite opposite to Silly Putty, in that they do exhibit solid-like behavior, even though their response is affected by the load rate. The magnetic interactions between the particles in this composite material depend on the magnetic orientation of each particle and their spatial relationship, which leads to an interesting number of magneto-mechanical phenomena (de Vicente et al., 2011; Ginder et al., 2000; Kallio, 2005). The aim of this work is to expand the applicability of MREs in engineering application like the more widespread magneto-responsive material: the magnetorheological fluids (MRFs) which exploit the same principle using a fluid matrix and are already used in many industrial applications, especially for vibration damping and shock absorbers (Carlson and Jolly, 2000; Chen et al., 2007; Shen et al., 2004; Spaggiari et al., 2016; Yang et al., 2015).

MREs include a large variety of composite materials, but their main components are always ferromagnetic particles immersed in a non-magnetic elastomeric matrix. The particles could be either a soft magnetic material, like Carbonyl Iron (Riesgo et al., 2019) or hard magnetic materials that retain the magnetization (Koo et al., 2012) and show a stronger anisotropicity. The constituents of MREs, the technologies for their manufacture and the mathematical models that best describe their mechanical properties present a range of very interesting scientific problems that are only partially treated in the scientific literature (Chen et al., 2007; Popp et al., 2009), especially regarding their mechanical properties in shear and up to failure. Compared to MRFs, magnetorheological elastomers always show solid behavior, that is, they do not pass from fluid to quasi-solid state, however their mechanical characteristics in terms of stiffness and damping are a function not only of the external mechanical loads, but also of the applied external magnetic field (Norouzi et al., 2016). Moreover, the change in the macroscopic properties of MREs is quite limited compared to MRFs (Kukla et al., 2017; Ruddy et al., 2008), but MREs are much more manageable than MRFs, which have the problems of confinement, compatibility with standard gaskets and can easily be damaged by the friction with magnetic particles (Güth et al., 2013; Spaggiari and Dragoni, 2012; Wiehe and Maas, 2012). One of the most important characteristics which make MREs different form MRFs is the possibility to obtain both isotropic and anisotropic configurations during the manufacturing of the samples, which is not possible with MRFs and the availability of hard magnetic materials to be used as particles. The particles within the elastomeric matrix can be homogeneously distributed forming isotropic MREs during the matrix cure, as shown in Figure 1(a), or they can be forced to form chain-like column structures, forming anisotropic MREs as shown in Figure 1(b) due to the application of an external magnetic field (Lian et al., 2015, 2018).

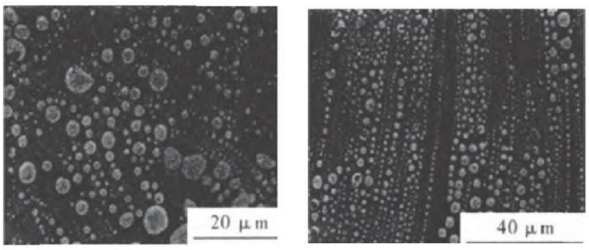

Figure 1. Microscopic structure of an MRE: (a) isotropic MRE, (b) anisotropic MRE (Lian et al., 2015).

The external magnetic field applied to the MRE induces dipolar moments in the ferromagnetic particles before the complete polymerization of the elastomer, so that the columnar structures of particles remain locked in place until the end of the cure, and then this structure is fixed in the matrix. Even though MREs can be used in different modes of operation such as tension/compression (Vatandoost et al., 2017), and shear mode, they are often used in shear behavior since it is quite easier to provide mechanical and magnetic loadings in perpendicular direction (Vatandoost et al., 2020). Several works in technical literature (Li, 2013; Popp et al., 2009) are devoted to assess the MREs properties, especially as a function of the shear rate, focusing mainly on cyclic tests but scarce information is provided about their behavior up to failure, therefore the aim of this paper is to provide further information about the shear properties of MREs up to failure, since this important feature helps in the MREs based devices design. Only few works tackles the fatigue properties (Calabrò, 2011; Zhou, 2016; Zhou et al., 2017) mostly in biaxial condition while it is difficult to find information on the ultimate shear strength of MRE. This paper therefore investigates a MRE made from a silicone-elastomeric matrix, a combination already studied in literature, (Bellelli and Spaggiari, 2019; Choi et al., 2018), by considering several weight fractions, the applied magnetic field and the isotropicity of the material, by testing it dynamically at several shear rates and also up to failure, in order to estimate the effect of the

variables on the material performance. A straightforward magneto-mechanical phenomenological model is proposed to estimate the behavior of the material in different conditions in terms of stiffness, ultimate shear stress and specific dissipated energy.

2. Materials and methods

The experimental tests were carried out following a Design of Experiment procedure (Montgomery, 2004). Three design variables are considered: weight fractions of ferromagnetic particles, specimen isotropicity and application of an external magnetic field during the test. For each configuration we manufactured two samples for a total of 14 specimens. Subsequently, we carried out shear tests, cyclic and up to failure both with and without an external magnetic field. [AQ: 2]

2.1. Experimental apparatus

The elastomeric matrix was obtained from a commercial PDMS (Polydimethylsiloxane) base, Sylgard 184, by Dow Corning, which is a two-component material which is widely used in electronic applications, especially for encapsulation of microelectronics circuits. This material shows very interesting properties as an electret and it was already described and studied in (Kachroudi et al., 2015), where its viscoelastic, thermal and dielectric properties can be found. The aim of this paper is to study and discuss its magnetorheological properties when enriched by various weight fractions of ferromagnetic particles. The elastomeric base was mixed with Carbonyl Iron Particles (CIP) with an average size of 45 μm, Ferchim RI 63/3.2 by Pometon (Italy). The three ingredients (curing agent, silicone base and CIP), after being weighted to obtain the desired weight fraction, were deposited and mixed. Since manual mixing of the components always introduces air inside the material, which is detrimental for the magneto-mechanical properties, first, a degassing procedure is carried out using a vacuum chamber at –0.8 Bar. Subsequently, the specimens were cast by pouring the material in a polymeric mold. The cylindrical specimens have a diameter of 15 mm and a height of 32 mm. We decided the specimens' dimensions based on the constraints given by the manufacturing method (mold and vacuum chamber volume) and the testing machine with magnetic yoke mounted on it. The mold, containing the reagents still in the liquid phase, was left for 15 min in the vacuum chamber for a second time to ensure a proper elimination of remaining air bubbles and then the curing step was started. Even though a long degassing is detrimental for the void formation in case of resin transfer molding technique (Woods et al., 2007) when the matrix is poured at room pressure and temperature, the void formation always happens due to mixing and only vacuum application is able to prevent this phenomenon, as verified in the post mortem analysis carried out after the failure tests.

The mold was placed in slow rotation through a stepper motor in order to avoid the settling of the iron particles due to the gravity and it was kept for 6 h in a climatic chamber at 45°C to ensure the complete polymerization of the elastomeric matrix. First, we manufactured the isotropic specimens with different weight fraction of ferromagnetic material (60%, 70%, 80%), creating two samples for each weight fraction considered. In order to produce the other six anisotropic specimens, two permanent magnets were placed around each specimen in the mold when the matrix was still uncured.

2.1.1. Magnetic system design. The effect of the magnetic field led to the formation of an aligned arrangement of particles inside the specimens. We estimated the magnetic field inside the mold and the yoke using a finite element model with FEMM software (Meeker, 2015). The magnetic field during the manufacturing was around 150 mT, Figure 2 shows the distribution inside the magnetic yoke used during the experimental tests. Figure 2(a) shows a regular distribution of the flux lines and, in the central part of the yoke used during the experimental tests, the induction field is around 300 mT on average (Figure 2(b)). Note that the central part of the yoke was considered as air, in order to allow for a comparison with the experimental measure. The magnetic induction field provided by the magnets, measured experimentally through a Gaussmeter GM05 by Hirst (in air), was around 260 mT, close enough to the numerical prediction and strong enough to produce a relevant effect on the MRE. Figure 3(a) shows the rotating system used to prevent CIP settling and the permanent magnets used on top and bottoms of the specimens to create the anisotropic specimens. Figure 3(b) shows the complete set of specimen used, including the last two control specimens of pure PDMS, with no ferromagnetic particles, which were manufactured to estimate the base material properties under the same test conditions of the magnetorheological samples.

The specimens were tested in shear tests both under cyclic and monotonic loading, as showed in Figure 4. The gap between the fork and the eye end is calibrated at 0.1 mm in order to be able to compute the shear stress in the MR elastomeric pin. While the cyclic tests at different shear rates were non-destructive and were carried out with the main aim to estimate stiffness and dissipated energy, the monotonic tests were performed up to failure, in order to assess the maximum shear stress. In the first case we limited the maximum applied displacement to 2 mm, which in any case guarantees a quite severe shear stress inside the pin without any permanent damage to the MRE. This limit value was chosen after a set of preliminary tests, not reported here

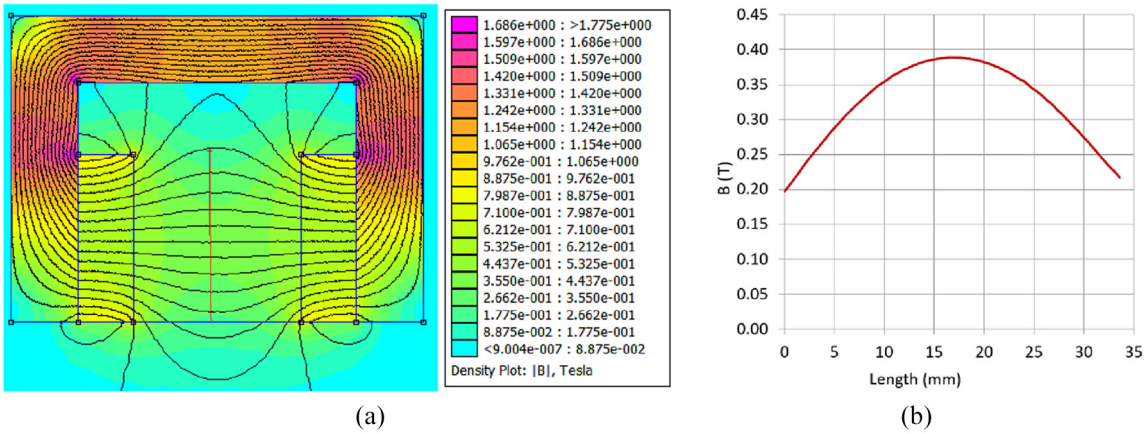

Figure 2. FEMM simulation: (a) flux lines and overall induction field, and (b) distribution in centre along the red line.

Figure 3. (a) Rotation system to prevent settlement of the particles, and (b) specimens manufactured.

Table 1. Specimens considered in the design plan.

Variable	Levels	Specimens						
CIP weight fraction	4	0	60		70		80	
Isotropicity	2	N/A	YES	NO	YES	NO	YES	NO
Replicates	2	2	2		2		2	
Total specimens	14	2	4		4		4	

for the sake of brevity. Three shear rates were considered in the cyclic test: 0.16, 0.83, 1.67 s^{-1}. The experimental plan included the execution of the cyclic and monotonic tests on 14 specimens. Table 1 reports a synthetic representation of the variables considered.

2.1.2. Shear test rig. The shear test equipment exploited a fork-pin-eye rig mounted between the clamps of the base and on the head of the test machine, a Galdabini Sun 500, equipped with a 5000 N load cell, as shown in Figure 4. Figure 4(a) shows the schematic of the loading in presence of the applied magnetic field, Figure 4(b) the specimen under test with no applied magnetic field and Figure 4(c) the application of the magnetic yoke. The specimen is held in position by precise coupling with the fork and the eye-rod, no adhesive is used to avoid any interference with the experimental results. The number of tests performed was 98: each of the 14 specimens was tested both in the absence and in the presence of an external magnetic field cycling the specimens at three shear rates and also in monotonic conditions. The external magnetic field was again obtained with two permanent magnets providing a quite uniform distribution larger than 200 mT, as showed in Figure 2(b). The load-displacement curves given by the universal testing system (UTS) machine were first transformed in shear strain vs shear stress and then used to compute the following quantities:

Figure 4. (a) Schematic of the test rig, (b) shear test set-up, and (c) test with permanent magnets on. The red dashed rectangle represents the MRE sample position.

- Shear modulus, computed as the slope of the first elastic part of the stress-strain curves (MPa)
- Failure shear stress for monotonic curves
- Specific dissipated energy (mJ/mm^3), for cyclic curves

The responses can be simply computed as follows. The shear stress is:

$$\tau = \frac{2F}{\pi d^2} \tag{1}$$

Where F is the experimental force and d is the MRE pin diameter. The shear strain can be computed both considering the engineering shear strain γ_{eng} or the true shear strain γ_{t}, defined as follows:

$$\gamma_{eng} = \frac{\Delta}{s} \tag{2}$$

$$\gamma_t = arctan\frac{\Delta}{s} \tag{3}$$

Where Δ is the experimental applied displacement and s is the gap between the fork and the eye-rod. According to the two definitions of shear strain, which has to be considered according to (Pardis et al., 2017) two possible formulations for the stiffness of the MRE are considered. The true shear strain is considered for the cyclic curves and used to compute the stiffness and the dissipated energy, according to the following expressions:

$$\gamma_t = \gamma_{0t} sin(\omega t), \tau = \tau_0 sin(\omega t + \delta) \tag{4}$$

$$\tau = \gamma_{0t} G' sin(\omega t) + \gamma_{0t} G'' cos(\omega t) \tag{5}$$

$$G_t^* = \frac{\tau_0}{\gamma_{0t}}(cos\delta + isin\delta) = \frac{\tau_0}{\gamma_{0t}} e^{i\delta} G = G' + iG'' \tag{6}$$

From which it is possible to separate the true storage modulus (G', real part) and the true loss modulus (G'', imaginary part). The engineering strain is used to describe the monotonic curves up to failure.

3. Experimental results

Figure 5(a) and (b) shows the shear stress versus engineering shear strain curves for isotropic specimens without the applied field (a) and with the field applied during the cyclic test (b). Figure 5(c) and (d) shows the curves for the anisotropic specimens without the applied field (c) and with the field applied during the cyclic test (c). t, for the three shear strain rates selected (0.167 s^{-1}, 0.833 s^{-1}, 1.67 s^{-1}).

The Payne effect (Clément et al., 2005) and the Mullin effect (Wang et al., 2015), which are quite typical for PDMS matrix with fillers, could affect the shear strain and the shear stress curves. The Payne effect can be a possible explanation for the shape of the curves reported in Figure 5, which shows non-linear behavior. In the low strain deformation region, the slope of the curves (identified as *G1*) is quite steep, while at sufficiently larger deformation, the slope (identified as *G2*) decreases, indicating a softening behavior. A simple bilinear regression of the stress-strain curves was used to identify parameters *G1* and *G2*, this simple method is used to allow the cyclic curves to be compared with the monotonic ones. Since these curves are mainly used to estimate the dissipated energy and the shear modulus

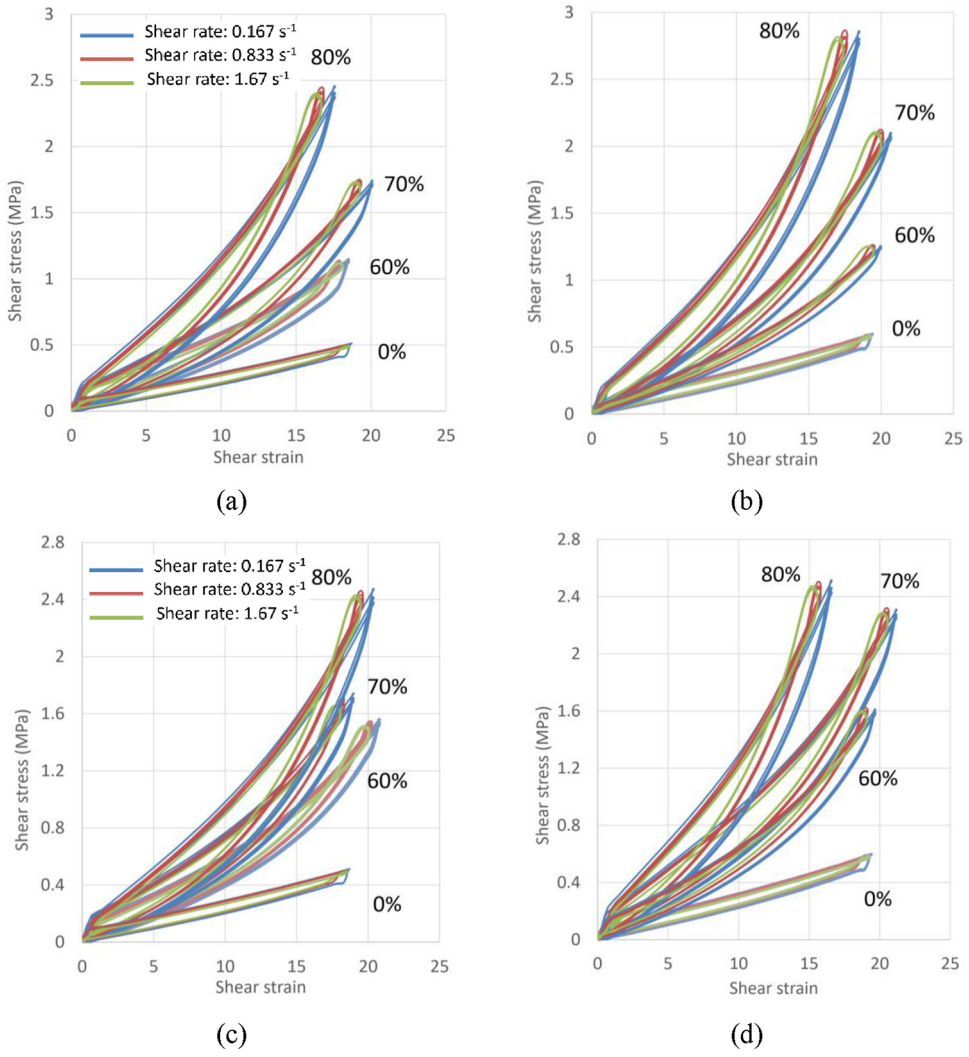

Figure 5. (a) Shear stress versus engineering shear strain curves on isotropic specimens, without, (b) and with the field applied, (c) and on anisotropic specimens, without, (d) and with the field applied.

the control mode was in speed, leading to a slightly different maximum shear strain.

Figure 6 shows the curves of the failure test of the specimens, for various weight fraction of ferromagnetic particles and for no applied magnetic field (Figure 6(a)) and applied magnetic field (Figure 6(b)). The behavior of the material is quite similar for isotropic and anisotropic specimen, therefore both isotropic and anisotropic are reported. The ANOVA analysis reported in the Discussion section confirms that the isotropicity does not affect the failure shear stress. All the experimental test of the specimens loaded up to failure are carried out controlling the displacement in quasi-static mode (1mm/min crosshead displacement). The difference between the pure PDMS specimen in case of magnetic field off and on it is imputable to a specimen difference, since with no CIP the intrinsic behaviour of the specimen should have been the same.

4. Discussion

The experimental cyclic tests were analyzed by evaluating the response of the material in terms of shear modulus and specific dissipated energy, while the destructive monotonic experimental tests were used to retrieve the maximum failure stress for the MRE specimens. A statistical software, Stat-Ease Design-Expert, (Anderson and Whitcomb, 2007) was used to verify the influence and interactions of the variables considered. The results were analyzed according to the variable plan shown in Table 1. Figures 7 and 8 show the half-normal diagrams of the four responses considered (Mead, 1990; Mead et al., 2012), useful for estimating the variables that have an influence on the response at a glance. The stronger the influence, the larger the distance from the error line, extrapolated from the green triangles, which represent the normal stochastic variation of an experimental test.

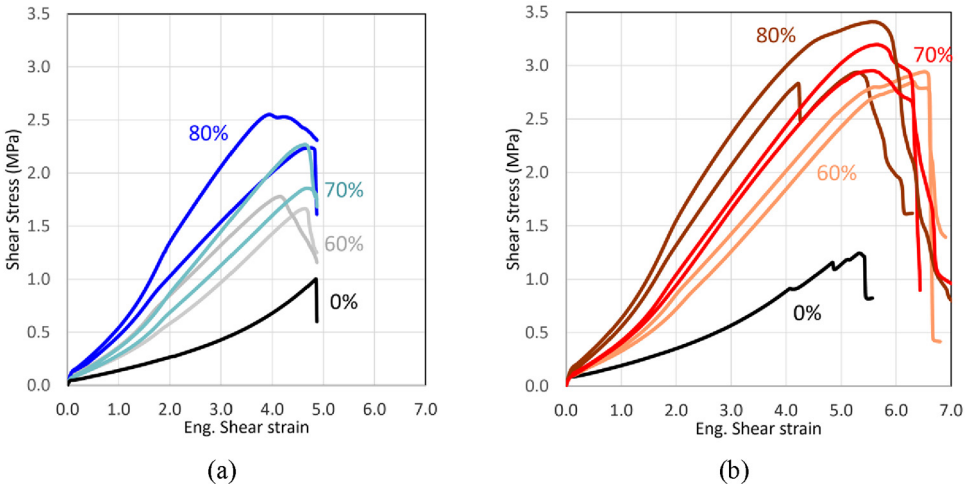

Figure 6. (a) Shear stress versus engineering strain curve of the specimens (both isotropic and anistropic) loaded up to failure with no magnetic field, and (b) with applied magnetic field.

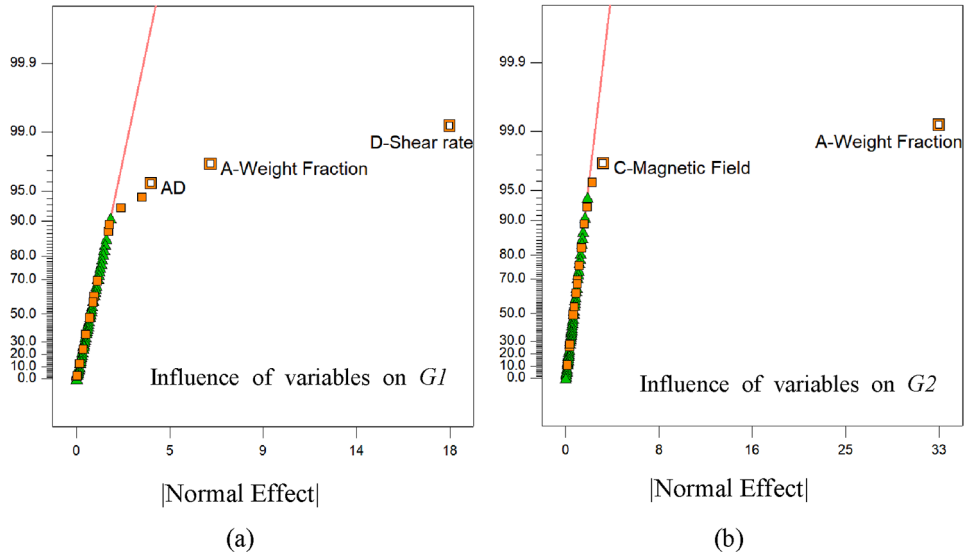

Figure 7. (a) Half-normal diagrams concerning the analysis of the shear modulus for small deformation, and (b) for large deformation.

Figure 7(a) reports the influence of the variable on the shear modulus at small strains, *G1*, Figure 7(b), on the shear modulus at large strains, *G2*, Figure 8(a) the influence on the specific dissipated energy, *E*, computed as the area below the cyclic curve and Figure 8(b) reports the influence of the variable on the failure shear stress, τ_{max}. This influence on the input variables is greater as they deviate from the error bar and the X-axis represents the influence on the response while the Y-axis expresses the confidence that the effect is not due to experimental noise.

Figure 7(a) and (b) reports the ANOVA for the shear modulus computed based on the cyclic tests. Since the deformations are quite large two different slopes can be computed. The first slope, *G1* is visible in Figure 5 for shear strain below 1, which corresponds to a vertical displacement of 0.1 mm, while the second slope, *G2*, which covers the vast majority of the plots in Figure 5, spans from 1 to 20 shear strain, which corresponds to a vertical displacement from 0.1 to 2 mm. Figure 7(a) shows that the initial slope *G1* is strongly affected by the shear rate, while the volume fraction and their interaction plays a minor role. This first part can be associated to the response of the viscoelastic matrix itself, which is known to be quite sensitive to the deformation rate. The ANOVA in Figure 7(a) shows that the most prominent variables are the shear rate and the weight fraction and also that there is a positive interaction between the two variables. Figure 7(b) shows that the most important variable for the slope in

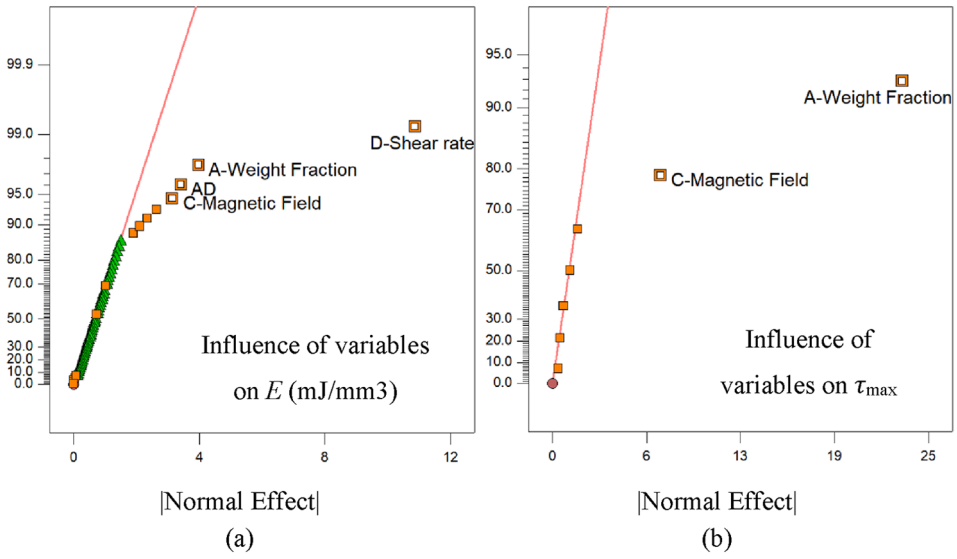

Figure 8. (a) Half-normal diagrams concerning the specific energy dissipated in cyclic test, and (b) maximum shear failure stress, from the monotonic tests.

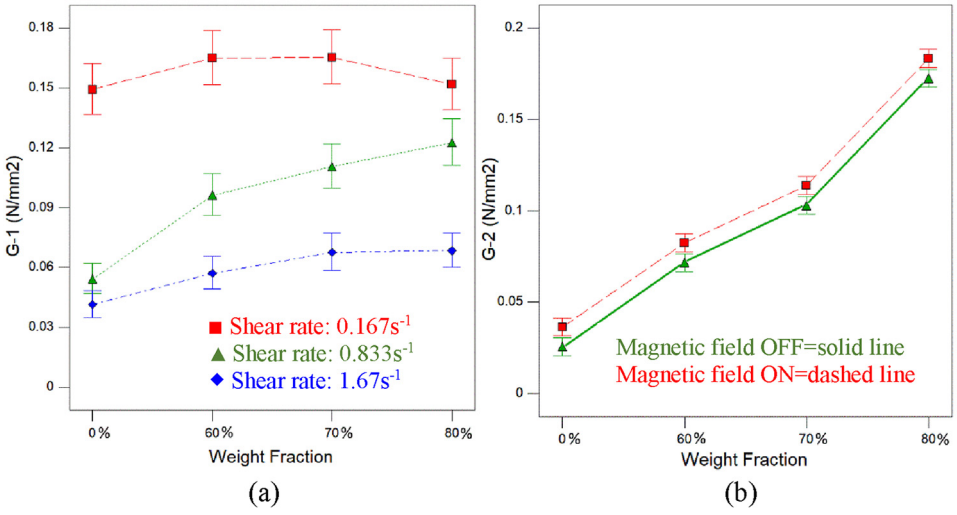

Figure 9. (a) Effect of the variables on the shear modulus at small deformation, and (b) at large deformations, under cyclic test.

large deformation is the weight fraction, with a slight influence of the applied magnetic field, which stiffens the system response.

Figure 8(a) reports the behavior of the system under cyclic load in terms of specific energy dissipated, E while the failure shear stress retrieved by the monotonic tests up to failure is reported in Figure 8(b). Figure 8(a) shows that the specific dissipated energy is sensitive to the shear rate mostly, but also to the weight fraction and to the applied magnetic field. The square AD in Figure 7(a), as well as in Figure 8(a), stands for the interaction between the weight fraction and the shear rate, indicating a non-linear effect of these two variable on the system response. Figure 8(b) reports the input variables which affect the tangential failure stress of the MRE and in this case, in addition to the weight fraction, there is a strong influence of the applied magnetic field, which is visible also in the plots of Figure 6. The shear stress increases with the magnetic field by roughly 50%, which opens the possibility of using MRE as a programmable material. The ANOVA not only highlights the important variables which affects the system response, but also provides qualitative information about their interactions and a quantitative phenomenological model. The interactions between the variables are reported in Figure 9(a) for the shear modulus at

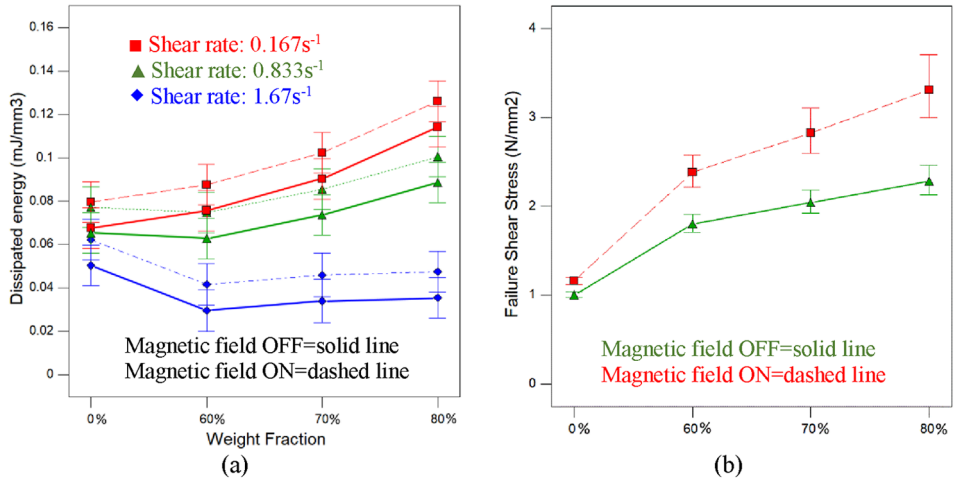

Figure 10. (a) Effect of the variables on the specific dissipated energy, (b) in cyclic test and on the maximum shear stress, in monotonic tests.

Table 2. ANOVA summary table.

	Increase in % weight	Increasing shear rate	Magnetic field presence	Anisotropicity
Stiffness, *G1* (MPa)	↑	↓ ↓ ↓	↑	x
Stiffness, *G2* (MPa)	↑ ↑ ↑	↑	↑	x
Dissipated energy (mJ/mm3)	↓	↓ ↓	↑	x
Failure shear stress (MPa)	↑ ↑	X	↑ ↑	x

small deformations and in Figure 9(b) for the shear modulus at large deformations. Figure 9 confirms the fact that it is important to separate the behavior, since for *G1* (Figure 9(a)) the most important effect is given by the shear rate, with a smaller contribution given by the weight fraction. Figure 9(b) shows that *G2* is dependent mostly on the particle concentration, with a slight effect of the magnetic field, which stiffens the MRE behavior regardless the shear rate.

Figure 10 show the interaction diagrams for the specific dissipated energy during the cyclic test (Figure 10(a)) and for the failure shear stress during the monotonic tests (Figure 10(b)). The situation depicted in Figure 10(a) is quite complex and shows that the shear rate affects strongly the dissipated energy, when the shear rate is low the dissipated energy increases, while the specimen stiffens and dissipates less energy at high shear rates. This behavior is confirmed also by considering the area under the curves in Figure 5, which becomes smaller with the increasing shear rates. A typical viscoelastic material shows an increase of the dissipative figures, such as the loss modulus, with a frequency increase, but this behavior is visible only in the high frequency range. Other researchers (Li and Nakano, 2013) found, in case of a PDMS based MRE, that the loss modulus, and therefore the dissipated energy, shows a decrease at low frequencies, which confirms our experimental findings.

The effect of the applied magnetic field is quite straightforward and acts as expected. The magnetic particles are affected by the magnetic field and the presence of the field (dashed lines in Figure 10) increases the dissipated energy for a given shear rate or weight fraction.

Figure 10(b) reports clearly the strong influence of both of the weight fraction and the magnetic field on the maximum shear stress, which could increase up to 50% in case of the higher weight fractions. This aspect could be exploited in several applications, which could be generalized under the broad category of programmable "mechanical fuse." The system could be as simple as the shear pin and fork used in the test, but designed to fail under excessive shear loads and protect components downstream one side of the system from excess of force (or even torque) in the event of a system jam. The possibility to control the shear stress could be exploited to adapt the system in real time to the external conditions in a fast and straightforward way.

A general recap of the experimental findings could be found in Table 2 where an ANOVA summary is reported, showing the influence of each individual factor on the analysed responses of the system. The results

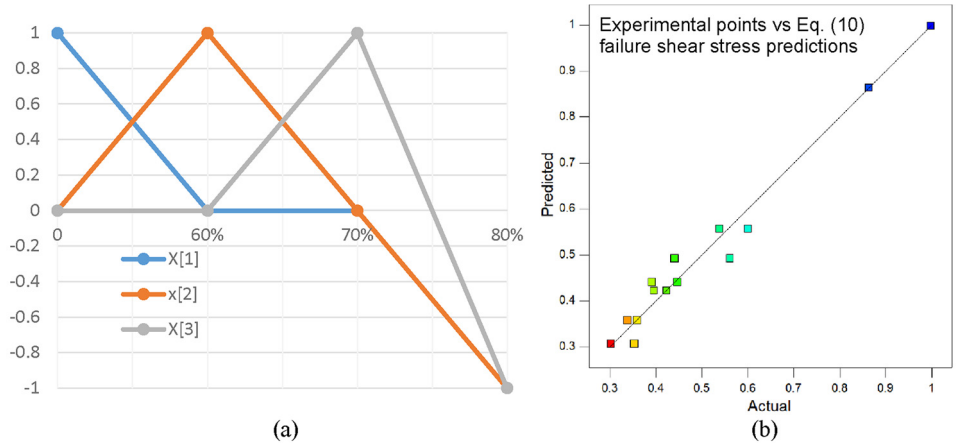

Figure 11. (a) Coded factors for a general three level variable *X*, and (b) accuracy of the proposed model of failure shear stress in terms of prediction and experimental points, with value normalized to 1.

are consistent with the findings of other researchers (Kukla et al., 2017; Schrittesser et al., 2009), but both confirm the stiffening effect of the ferromagnetic particles especially at high weight fractions and large strains and the controllability of the material is confirmed even for the failure shear stress. The ANOVA performed on the data could be also exploited to build a simple phenomenological model, based on the four-input variable considered, the weight fraction (A), the isotropicity (B), the applied magnetic field (C) and the shear rate (D). The predictive models were obtained for each response of the system. The proposed models are expressed in equation (7) for the stiffness *G1*, in equation (8) for *G2*, (both expressed in MPa), in equation (9) for the specific dissipated energy, *E*, expressed in J/dm^3 and in equation (10) for the failure shear stress, τ_{max}. The software linearizes the responses and to do so it applies a so-called transformation whenever useful as for the *G1* (square root), *G2* (inverse square root) and for the failure shear stress (inverse). The expressions below are reported using coded factors, a compact form used to express the levels of the variables considered. Figure 11(a) shows the graphical meaning of the coded factors X[i] considered, which are used to represent all the possible levels of ferromagnetic particles (A[i]) and shear rates (D[i]), from the lower level to the higher one. The magnetic field applied is simpler (field ON $\rightarrow C = -1$, field OFF $\rightarrow C = 1$). Once the desired configuration is chosen, the prediction can be done. The comparison of the prediction and the model is reported in Figure 11(b), with the model (Y-Axis) and the experimental results (X-Axis) for the failure shear stress as example. The predicted failure shear stress (Y-axis), obtained through equation (10), is compared with the experimental values in Figure 11(b). The closer the points are to the 45° line, the better the model prediction. The agreement seems quite good, considering the simple phenomenological model adopted.

$$G1(MPa) = (0.31 - 0.041 \cdot A[1] + 0.018 \cdot A[3] + 0.083 \cdot D[1] + 0.03 \cdot A[1]D[1] - 0.033 \cdot A[1]D[2])^2 \quad (7)$$

$$G2(MPa) = 0.1 - 0.068 \cdot A[1] - 0.022 \cdot \mathrm{A}[2] + 0.009856 \cdot \mathrm{A}[3] - 0.00541 \cdot \mathrm{C} \quad (8)$$

$$E\left(\frac{J}{dm^3}\right) = \begin{pmatrix} 71.73 - 4.64 \cdot A[1] - 9.68 \cdot A[2] + 5.87 \cdot \mathrm{C} + 21.24 \cdot \mathrm{D}[1] + 6.87 \cdot \mathrm{D}[2] \\ -14.6 \cdot \mathrm{A}[1]\mathrm{D}[1] - 1.62 \cdot \mathrm{A}[2]\mathrm{D}[1] + 2.75 - 14.67 \cdot \mathrm{A}[3]\mathrm{D}[1] - 2.65 \cdot \mathrm{A}[1]\mathrm{D}[1] \end{pmatrix} \cdot 94.23 \quad (9)$$

$$\tau_{max}(\mathrm{MPa}) = \frac{3.308}{(0.55 + 0.38 \cdot A[1] - 0.065 \cdot A[2] - 0.13 \cdot A[3] + 0.7 \cdot \mathrm{C})} \quad (10)$$

An example on how to exploit the provided models is reported for the sake of clarity. The hypothesis is that one would like to predict the failure shear stress of a 75% specimen with no magnetic field applied. The equations provided would give the result reported in equation (11), which is in good agreement with experimental tests shown in Figure 10(b).

$$\tau_{max} = \frac{3.308}{(0.55 + 0.38 \cdot (-0.5) - 0.065 \cdot (-0.5) - 0.13 \cdot 0 + 0.7 \cdot 1)} = 3.0279MPa \quad (11)$$

5. Conclusion

This work analyzes the shear behavior of an MR elastomer up to failure, for a wide range of particles weight fractions and test conditions. The experimental tests show that the not only the composition of the MRE strongly affects the MRE behavior in term of stiffness, but also that the magnetic field is strongly interacting in enhancing the MRE failure shear stress. The positive effect of the weight fraction on the shear modulus is more evident when large deformations are considered. The specific energy dissipated by the material is mainly controlled by the applied shear rate, as expected, but also the applied magnetic field is quite relevant in changing the dissipated energy. In general, the influence of the anisotropy in the specimen is not predominant, due to the fact that the particle alignment and loading direction are perpendicular. A quite interesting outcome of this research is the strong dependence of the failure shear stress on the external magnetic field, which open new possibilities in terms of exploiting the material as a "programmable mechanical fuse" which changes its threshold failure stress value based on the applied magnetic field. Simple phenomenological models are also provided for all the outputs considered, based on the input variables. The proposed models, despite their simplicity, are able to provide a reasonable estimate of the material behavior, and thus they could be directly applicable for design purposes.

Acknowledgements

The authors would like to acknowledge Dr. Luke Mizzi for the help in revising this work and the fruitful discussion and Mr. Francesco Morandi for the help in the experimental manufacturing of the specimens.

Declaration of conflicting interests

The authors declared no potential conflicts of interest with respect to the research, authorship, and/or publication of this article.

Funding

The authors received no financial support for the research, authorship, and/or publication of this article.

ORCID iD

Andrea Spaggiari https://orcid.org/0000-0001-8959-2599

References

Anderson MJ and Whitcomb PJ (2007) *DOE Simplified: Practical Tools for Effective Experimentation, Second Edition*. 2 ed. Productivity Press. [AQ: 3]

Bellelli A and Spaggiari A (2019) Magneto-mechanical characterization of magnetorheological elastomers. *Journal of Intelligent Material Systems and Structures* 30(17): 2534–2543.

Calabrò R (2011) Mechanical characterization of elastomers under quasi-static and dynamic biaxial loading conditions. 196. [AQ: 4]

Carlson JD and Jolly MR (2000) MR fluid, foam and elastomer devices. *Mechatronics* 10(4–5): 555–569.

Chen L, Gong XL and Li WH (2007) Microstructures and viscoelastic properties of anisotropic magnetorheological elastomers. *Smart Materials and Structures* 16(6): 2645–2650.

Choi YT, Hartzell CM, Leps T, et al. (2018) Gripping characteristics of an electromagnetically activated magnetorheological fluid-based gripper. *AIP Advances* 8(5): 056701.

Clément F, Bokobza L and Monnerie L (2005) Investigation of the payne effect and its temperature dependence on silica-filled polydimethylsiloxane networks. Part I: experimental results. *Rubber Chemistry and Technology* 78(2): 211–231.

Cross R (2012) Elastic and viscous properties of Silly Putty. *American Journal of Physics* 80(10): 870–875.

Davis LC (1999) Model of magnetorheological elastomers. *Journal of Applied Physics* 85(6): 3348.

de Vicente J, Klingenberg DJ and Hidalgo-Alvarez R (2011) Magnetorheological fluids: a review. *Soft Matter* 7(8): 3701.

Eem SH, Koo JH and Jung HJ (2019) Feasibility study of an adaptive mount system based on magnetorheological elastomer using real-time hybrid simulation. *Journal of Intelligent Material Systems and Structures* 30(5): 701–707.

Ginder JM, Nichols ME, Elie LD, et al. (2000) Controllable-stiffness components based on magnetorheological elastomers. *SPIE's 7th Annual International Symposium on Smart Structures and Materials* 3985: 418–425.

Golinelli N, Spaggiari A and Dragoni E (2015) Mechanical behaviour of magnetic Silly Putty: Viscoelastic and magnetorheological properties. *Journal of Intelligent Material Systems and Structures*: 1045389X15591655-epub ahead of print July, 8 2015. DOI: 10.1177/1045389X15591655.[AQ: 5]

Guan X, Dong X and Ou J (2008) Magnetostrictive effect of magnetorheological elastomer. *Journal of Magnetism and Magnetic Materials* 320(3–4): 158–163.

Güth D, Wiebe A, Maas J, et al. (2013) Design of shear gaps for high-speed and high-load MRF brakes and clutches. *Journal of Physics: Conference Series* 412(1): 012046.

Kachroudi A, Basrour S, Rufer L, et al. (2015) Piezoelectric cellular micro-structured PDMS material for microsensors and energy harvesting. *Journal of Physics: Conference Series* 660(1): 012040.

Kallio M (2005) *The elastic and damping properties of magnetorheological elastomers*. [PhD Thesis]. Vtt Publications. VTT Technical Research Centre of Finland.

Kim SH, Park YJ, Cha AR, et al. (2018) A feasibility work on the applications of MRE to automotive components. In: *IOP Conference Series: Materials Science and Engineering*, 6 April. Bristol, UK: Institute of Physics Publishing. DOI: 10.1088/1757-899X/333/1/012013.

Koo JH, Dawson A and Jung HJ (2012) Characterization of actuation properties of magnetorheological elastomers with embedded hard magnetic particles. In: *Journal of Intelligent Material Systems and Structures* 23(9): 1049–1054.

Kukla M, Górecki J, Malujda I, et al. (2017) The determination of Mechanical Properties of Magnetorheological Elastomers (MREs). *Procedia Engineering* 177: 324–330.

Li W and Zhang X (2012) Research and applications of MR elastomers. *Recent Patents on Mechanical Engineeringe* 1(3): 161–166.

Li WH and Nakano M (2013) Fabrication and characterization of PDMS based magnetorheological elastomers. *Smart Materials and Structures* 22(5): 055035.

Li YL, Li J, Tian T and Li W (2013) A highly adjustable magnetorheological elastomer base isolator for applications of real-time adaptive control. *Smart Materials and Structures* 22(9): 095020. [AQ: 6]

Lian C, Lee K-H and Lee C-H (2015) Friction and wear characteristics of magneto-rheological elastomers based on silicone/polyurethane hybrid. *Journal of Tribology* 137(3): 031607.

Lian C, Lee KH, Choi SB, et al. (2018) A study of the magnetic fatigue properties of a magnetorheological elastomer. *Journal of Intelligent Material Systems and Structures* 30(5): 1–6.

Marc Hartzman (2013) A touch of knowledge: the very serious history of Silly Putty. *HuffPost*. Available at: https://www.huffingtonpost.com/marc-hartzman/a-touch-of-knowledge-the-_2_b_1308405.html?guccounter=1 (accessed 13 September 2018).

Mead R (1990) *The Design of Experiments: Statistical Principles for Practical Applications*. Cambridge University Press. Available at: https://books.google.com/books?hl=it&lr=&id=CaFZPbCllrMC&pgis=1 (accessed 3 November 2015). [AQ: 7]

Meeker D (2015) FEMM 4.2 - Finite element method magnetics homepage. Available at: http://www.femm.info/Archives/doc/manual42.pdf (accessed 6 October 2016).

Montgomery DC (2004) Design and Analysis of Experiments. *Design and Analysis of Experiments*. Wiley: John Wiley and Sons.

Norouzi M, Sajjadi Alehashem SM, Vatandoost H, et al. (2016) A new approach for modeling of magnetorheological elastomers. *Journal of Intelligent Material Systems and Structures* 27(8): 1121–1135.

Pardis N, Ebrahimi R and Kim HS (2017) Equivalent strain at large shear deformation: Theoretical, numerical and finite element analysis. *Journal of Applied Research and Technology* 15(5): 442–448.

Popp KM, Zhang XZ, Li WH, et al. (2009) MRE properties under shear and squeeze modes and applications. *Journal of Physics: Conference Series* 149: 012095. DOI: 10.1088/1742-6596/149/1/012095.

Mead R, Gilmour SG and Mead A. (2012) Statistical principles for the design of experiments: applications to real experiments. Available at: http://www.amazon.com/Statistical-Principles-Design-Experiments-Probabilistic/dp/0521862140 (accessed 3 November 2015).

Riesgo G, Elbaile L, Moriche R, et al. (2019) Influence of the remnant magnetization, size distribution and content of soft magnetic reinforcement in micro-mechanical behavior of polymer matrix composites. *Polymer Testing* 79: 106020.

Ruddy C, Ahearne E and Byrne G (2008) A review of magnetorheological elastomers: properties and applications. Available at: http://www.ucd.ie/mecheng/ams/news_items/Cillian Ruddy.pdf (accessed 8 March 2017).

Schrittesser B, Major Z and Filipcsei G (2009) Characterization of the dynamic mechanical behavior of magneto – elastomers. *Journal of Physics: Conference Series* 149: 012096. DOI: 10.1088/1742-6596/149/1/012096.

Shen Y, Golnaraghi MF and Heppler GR (2004) Experimental research and modeling of magnetorheological elastomers. *Journal of Intelligent Material Systems and Structures* 15(1): 27–35.

Spaggiari A and Dragoni E (2012) Efficient dynamic modelling and characterization of a magnetorheological damper. *Meccanica* 47(8): 2041–2054.

Spaggiari A, Castagnetti D, Golinelli N, et al. (2016) Smart materials: properties, design and mechatronic applications. *Proceedings of the Institution of Mechanical Engineers, Part L: Journal of Materials: Design and Applications* 0(0): 1–29.

Vatandoost H, Norouzi M, Alehashem SMS, et al. (2017) A novel phenomenological model for dynamic behavior of magnetorheological elastomers in tension–compression mode. *Smart Materials and Structures* 26(6): 065011.

Vatandoost H, Hemmatian M, Sedaghati R, et al. (2020) Dynamic characterization of isotropic and anisotropic magnetorheological elastomers in the oscillatory squeeze mode superimposed on large static pre-strain. *Composites Part B: Engineering* 182: 107648. DOI: 10.1016/j.compositesb.2019.107648.

Wang Z, Li S, Wei D, et al. (2015) Mechanical properties, Payne effect, and Mullins effect of thermoplastic vulcanizates based on high-impact polystyrene and styrene–butadiene rubber compatibilized by styrene–butadiene–styrene block copolymer. *Journal of Thermoplastic Composite Materials* 28(8): 1154–1172.

Wiehe A and Maas J (2012) Large-scale test bench for the durability analysis of magnetorheological fluids. *Journal of Intelligent Material Systems and Structures* 24(12): 1433–1444.

Woods BKS, Wereley N, Hoffmaster R, et al. (2007) Manufacture of bulk magnetorheological elastomers using vacuum assisted resin transfer molding. *International Journal of Modern Physics B* 21(28–29): 5010–5017.

Yang C, Fu J, Yu M, et al. (2015) A new magnetorheological elastomer isolator in shear–compression mixed mode. *Journal of Intelligent Material Systems and Structures* 26(10): 1290–1300.

Zhou Y (2016) *Fatigue Properties of Magnetorheological Elastomers And The Design Of Interfacial Layers To Improve Fatigue Life*. Dublin Institute of Technology. DOI: 10.21427/D75315.[AQ: 8]

Zhou Y, Johnson M, Wen S, et al. (2017) Equi-biaxial fatigue behaviour of magnetorheological elastomers in magnetic fields. *Journal of Intelligent Material Systems and Structures* 28(5): 687–696.